WASP-4b Arrived Early for the TESS Mission

L. G. BOUMA,[1] J. N. WINN,[1] C. BAXTER,[2] W. BHATTI,[1] T. DAYLAN,[3] J.-M. DÉSERT,[2] M. HILL,[4] S. KANE,[4] K. G. STASSUN,[5, 6]
G. R. RICKER,[3] R. VANDERSPEK,[3] D. W. LATHAM,[7] S. SEAGER,[8] J. M. JENKINS,[9] Z. BERTA-THOMPSON,[10] D. A. CALDWELL,[9, 11]
K. COLÓN,[12] M. FAUSNAUGH,[3] A. GLIDDEN,[3] N. GUERRERO,[3] J. RODRIGUEZ,[7] J. D. TWICKEN,[9, 11] AND B. WOHLER[9, 11]

[1] Department of Astrophysical Sciences, Princeton University, 4 Ivy Lane, Princeton, NJ 08540, USA
[2] API, University of Amsterdam, P.O. Box 94249, 1090 GE Amsterdam, The Netherlands
[3] Department of Physics and Kavli Institute for Astrophysics and Space Research, Massachusetts Institute of Technology, Cambridge, MA 02139, USA
[4] Department of Earth Sciences, University of California, Riverside, CA 92521, USA
[5] Vanderbilt University, Department of Physics & Astronomy, 6301 Stevenson Center Lane, Nashville, TN 37235, USA
[6] Fisk University, Department of Physics, 1000 17th Avenue N., Nashville, TN 37208, USA
[7] Harvard-Smithsonian Center for Astrophysics, 60 Garden Street, Cambridge, MA 02138, USA
[8] Department of Earth, Atmospheric, and Planetary Sciences, Massachusetts Institute of Technology, Cambridge, MA 02139, USA
[9] NASA Ames Research Center, Moffett Field, CA 94035, USA
[10] Department of Astrophysical and Planetary Sciences, University of Colorado, Boulder, CO 80309, USA
[11] SETI Institute, Mountain View, CA 94043, USA
[12] NASA Goddard Space Flight Center, Exoplanets and Stellar Astrophysics Laboratory (Code 667), Greenbelt, MD 20771, USA

ABSTRACT

The Transiting Exoplanet Survey Satellite (TESS) recently observed 18 transits of the hot Jupiter WASP-4b. The sequence of transits occurred 81.5 ± 11.7 seconds earlier than had been predicted, based on data stretching back to 2007. This is unlikely to be the result of a clock error, because TESS observations of other hot Jupiters (WASP-6b, 18b, and 46b) are compatible with a constant period, ruling out an 81.5-second offset at the 6.4σ level. The 1.3-day orbital period of WASP-4b appears to be decreasing at a rate of $\dot{P} = -12.6 \pm 1.2$ milliseconds per year. This might be caused by tidal orbital decay or apsidal precession, although both interpretations have shortcomings. The gravitational influence of a third body is another possibility, although at present there is no evidence for such a body. Further observations are needed to confirm and understand the timing variation.

Keywords: planet-star interactions — planets and satellites: individual (WASP-4b, WASP-5b, WASP-6b, WASP-12b, WASP-18b, WASP-46b) — binaries: close

1. INTRODUCTION

Although the Transiting Exoplanet Survey Satellite (TESS) is designed to detect new planets, it will also perform precise photometric monitoring of most of the planets that have been discovered by ground-based transit surveys over the last two decades. One of the applications of the new TESS data is to search for timing anomalies in hot Jupiter systems. Long-term monitoring of hot Jupiter transit and occultation times should eventually reveal two distinct processes.

First, whenever the orbital angular momentum is less than 3 times the rotational angular momentum, the system is vulnerable to tidal orbital decay (Counselman 1973; Hut 1980).

Corresponding author: L. G. Bouma
luke@astro.princeton.edu

Most hot Jupiters satisfy this condition and their orbits should be shrinking (Levrard et al. 2009; Matsumura et al. 2010). The rate of decay, which depends on how friction dissipates the energy of tidal disturbances, is difficult to observe directly or calculate from first principles. This has been a stubborn source of uncertainty in the interpretation of many phenomena in stellar and planetary astrophysics (as reviewed by Mazeh 2008 and Ogilvie 2014).

Second, long-term timing studies may reveal apsidal precession, *i.e.*, the rotation of the orbital ellipse within the orbital plane. Apsidal precession has long been observed in eclipsing binaries (*e.g.*, Schwarzschild 1958; Torres et al. 2010; Borkovits et al. 2015). For exoplanets, precessing orbits have been detected in a handful of cases, including circumbinary systems (Kepler-413 Kostov et al. 2014; Kepler-453 Welsh et al. 2015, planets orbiting rapidly rotating stars (Kepler-13 Szabó et al. 2012, 2014, Masuda 2015;

and systems with multiple interacting giant planets (Kepler-108 Mills & Fabrycky 2017; Kepler-693 Masuda 2017). Apsidal precession is not regularly observed in hot Jupiter systems because their orbits are nearly circular, which may itself be a consequence of star-planet tides. If it could be observed, then Ragozzine & Wolf (2009) showed that it would be possible to measure the planet's Love number, which would be a valuable constraint on the planet's interior.

So far, the most convincing direct evidence for either orbital decay or apsidal precession has come from WASP-12b. Maciejewski et al. (2016) and Patra et al. (2017) showed that the transit period of WASP-12b has been steadily decreasing by about 30 milliseconds per year over the last decade. Here, we present evidence for a timing anomaly in the WASP-4 system. The hot Jupiter WASP-4b orbits a G7V star every 1.34 days, corresponding to an orbital distance of 5.5 stellar radii (Wilson et al. 2008; Hoyer et al. 2013). It is a good target to search for departures from a constant period, because transit data exists all the way back to 2007. The orbital eccentricity is less than 0.018 (2σ), based on the work of Knutson et al. (2014), who combined the available transit times, occultation times, and Doppler data. The stellar obliquity (or at least its sky projection) is also compatible with zero, within about 10 degrees (Triaud et al. 2010; Beerer et al. 2011; Sanchis-Ojeda et al. 2011).

In what follows, § 2 presents the new TESS observations, and § 3 describes our timing analysis. We tried fitting the data with three models: a constant period, a decaying period, and a slightly eccentric precessing orbit. A constant period can be ruled out, but we cannot distinguish between the latter two possibilities. Either possibility would have interesting implications, described in § 4. Appendix A considers the possibility that the WASP-4 timing anomaly is due to an error in time stamps in the TESS data products. We found this possibility to be unlikely because none of the other hot Jupiters we examined show a timing offset with the same amplitude as was seen for WASP-4.

2. NEW TRANSITS AND SYSTEM PARAMETERS

2.1. *Observations*

WASP-4 was observed by TESS with Camera 2 from August 23 to September 20, 2018, within the second "sector" of science operations. The star is designated as TIC 402026209 in the TESS Input Catalog (Stassun et al. 2018). The pixel data for an 11×11 array surrounding WASP-4 were averaged into 2-minute stacks by the onboard computer. The data were downlinked via the Deep Space Network. The timestamps from the spacecraft clock were then transformed by the Payload Operations Center into the *Temps Dynamique Barycentrique* (TDB) reference system. The images were then reduced to lightcurves by the Science Processing Operations Center (SPOC) at NASA Ames (Jenkins et al. 2016). During this processing, the SPOC used the known spacecraft trajectory to compute the barycentric time corrections on a target by target basis, and expressed the timestamps as Barycentric TESS Julian Dates (BTJD), which is simply the barycentric Julian date minus 2,457,000. The lightcurves were vetted
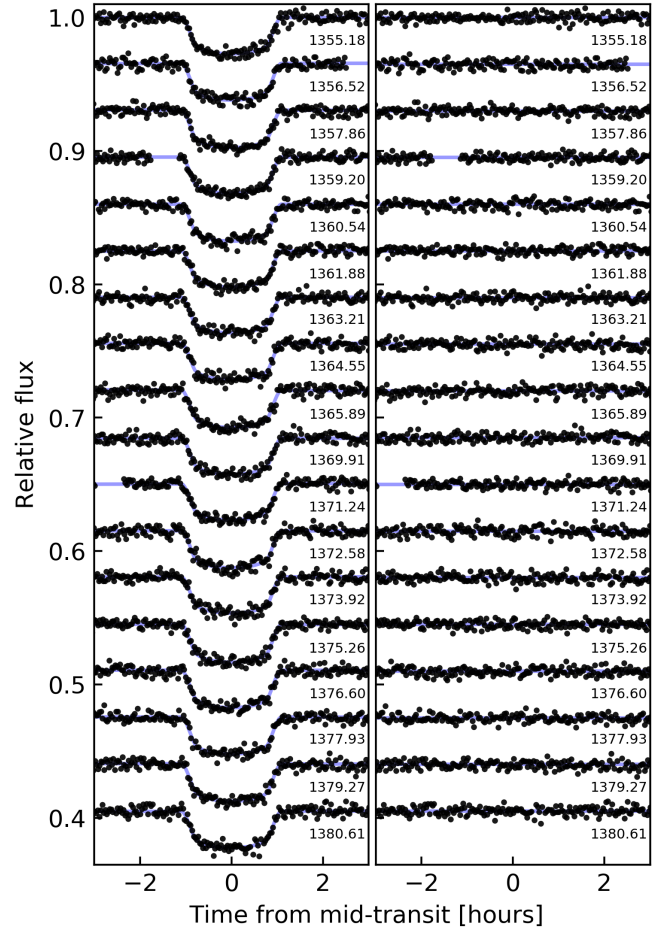

Figure 1. TESS observations of WASP-4b. On the left, black points are TESS flux measurements, with a vertical offset applied. Blue curves are best-fit models. The numbers printed next to each lightcurve are the approximate transit times expressed in BJD minus 2,457,000. The right side shows the residuals.

and released by the MIT TESS Science Office to the Mikulski Archive for Space Telescopes on November 29, 2018 (Ricker & Vanderspek 2018).

We began our analysis with the Presearch Data Conditioning (PDC) lightcurve (Smith et al. 2017a,b). We processed the lightcurve as follows. First, we removed all points with non-zero quality flags. This removed data contaminated by coarse spacecraft pointing, cosmic rays, and other annoyances (Mansouri-Samani et al. 2018). We also removed the data within the first and last hours of both orbits, because of ramp-like systematic effects that appear during those time ranges. We also removed the data that might have been adversely affected by "momentum dumps," the firing of thrusters and resetting of reaction wheels[1] that took place every 2.5 days during sector 2. The data during these

[1]   archive.stsci.edu/hlsps/tess-data-alerts/hlsp_tess-data-alerts_tess_phot_s01_tess_v1_release-notes.pdf
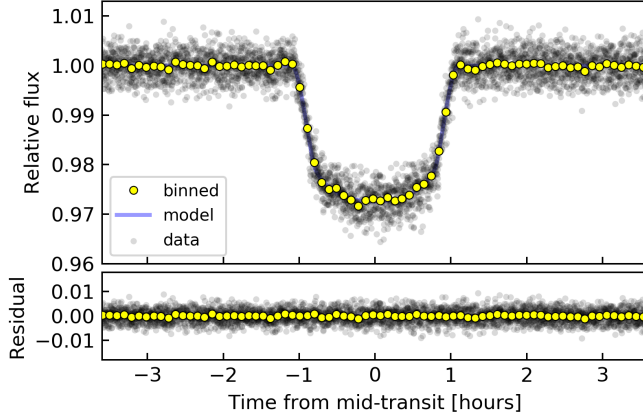
Figure 2. Phase-folded lightcurve of WASP-4b. Black points are TESS data. Yellow points are binned measurements. The bottom panel shows the residuals. The fit to the phase-folded transit (blue line) is used when measuring mid-transit times for the individual transits (see text).

events were assigned quality flags corresponding to "Reaction Wheel Desaturation Event" and "Manual Exclude". For WASP-4, these flags were simultaneously set for 54 distinct cadences, and there were 10 momentum dumps, averaging about 10 minutes of flagged data per dump. Out of caution, we clipped out an additional 10 minutes before and after every momentum dump.

All told, we removed 8% of the original data points, and were left with 18,165 measurements of the relative flux of WASP-4. We normalized the data by dividing out the median flux. We converted the timestamps from BTJD into BJD by adding the appropriate 2457000 day offset (Mansouri-Samani et al. 2018). Many of these and subsequent processing steps were performed using `astrobase` (Bhatti et al. 2018). We did not "flatten" the lightcurves, as is often done with splines, polynomials, or Gaussian processes. Instead, we modeled the out-of-transit flux variations simultaneously with the transit parameters, as described below.

2.2. *Measuring the transit times*

Using the cleaned PDC lightcurve, we used the Box Least Squares algorithm (Kovács et al. 2002) to estimate the orbital period, transit duration, and a reference epoch using the TESS data alone. Based on the results, we isolated the data within 4 transit durations of each transit midpoint. To find the transit parameters that best fit the data, we first fitted a line to the out-of-transit flux measurements surrounding each transit, and divided it out. We then created a phase-folded lightcurve and fitted a standard transit model using the analytic formulae given by Mandel & Agol (2002) and implemented by Kreidberg (2015). We assumed the orbit to be circular. The free parameters were the reference epoch, the planet to star radius ratio $R_p/R_\star$, the orbital distance to stellar radius ratio $a/R_\star$, the inclination i, two quadratic limb-darkening coefficients (u_{linear}, u_{quad}), and the orbital period P.

We sampled the posterior probability distribution for all the parameters using the algorithm proposed by Goodman & Weare (2010) and implemented by Foreman-Mackey et al. (2013). Table 1 gives the results, which are in reasonable agreement with the parameters reported by *e.g.*, Southworth et al. (2009) and Huitson et al. (2017). Figure 2 shows the phase-folded lightcurve.

To measure the transit times, we returned to the 'cleaned' PDC time series and fitted the data surrounding each transit separately, with four free parameters: the time of mid-transit t_{tra}, the planet-to-star radius ratio, and the slope and intercept of a linear trend to account for any slow variations unrelated to the transit. We fixed the remaining parameters at the values that had been determined from the phase-folded TESS lightcurve. The uncertainty in each data point was set equal to the root-mean-square (rms) level of the out-of-transit data.

To verify that the measured uncertainties are plausible, we computed the reduced χ^2 for a linear ephemeris fit to the measured TESS transit times. We found that $\chi^2 = 9.2$, with $n = 16$ degrees of freedom. The variance of the χ^2 distribution is $2n$, so we would expect $\chi^2 = 16 \pm 5.7$. Visually inspecting the residuals showed that the error variance had been overestimated, so we multiplied the measured TESS errors by a factor $f = 0.76$, forcing a reduced χ^2 of unity. This lowered the mean uncertainty of the transit midtimes from 29.8 to 22.6 seconds. We verified that omitting this step did not appreciably alter any of our conclusions.

Figure 1 shows the lightcurve of each transit, the best-fit models, and the residuals. Table 2 reports the mid-transit times and their uncertainties. After binning the residuals to 1-hour windows, the lightcurves have an rms scatter of 586 ppm. The pre-launch TESS noise model[2] (Winn 2013; Sullivan et al. 2015) would have predicted an error budget consisting of the following terms added in quadrature: 410 ppm from photon-counting noise, 202 ppm from detector read noise, and 673 ppm from the zodiacal background light. The level of background light appears to have been overestimated.

2.3. *Star and planet parameters*

We calculated the stellar and planetary parameters in the following way. We computed the star's spectral energy distribution based on the *Gaia* DR2 parallax (after making the small correction advocated by Stassun & Torres 2018) and the broadband magnitudes from the available all-sky catalogs: G from *Gaia* DR2, B_T and V_T from *Tycho-2*, $BVgri$ from *APASS*, JHK_S from *2MASS*, and the *WISE* 1–4 passbands, thus spanning the wavelength range 0.4–22 μm. We adopted the effective temperature from the work by Doyle et al. (2013), who determined the spectroscopic parameters of WASP-4 using high-signal-to-noise observations with the High Accuracy Radial-velocity Planet Searcher (HARPS). Then, we determined the stellar radius through the combination of the bolometric luminosity and the effective temper-

---

[2] github.com/lgbouma/tnm

Table 1. Selected system parameters of WASP-4b

Parameter	Value	68% Confidence Interval	Comment
Transit/RV parameters:			
$R_{\rm p}/R_\star$	0.15201	+0.00040, −0.00033	A
i [deg]	89.06	+0.65, −0.84	A
$a/R_\star$	5.451	+0.023, −0.052	A
$u_{\rm linear}$	0.382	—	A
$u_{\rm quad}$	0.210	—	A
K [m s^{-1}]	241.1	+2.8, −3.1	B
Stellar parameters:			
$T_{\rm eff}$ [K]	5400	±90	C
$\log g_\star$ [cgs]	4.47	±0.11	C
[Fe/H]	−0.07	±0.19	C
$F_{\rm bol}$ [erg cm^{-2} s^{-1}]	2.802×10^{-10}	$\pm 0.076 \times 10^{-10}$	D
π [mas]	3.7145	0.0517	F
$R_\star$ [R$_\odot$]	0.893	±0.034	E
$\rho_\star$ [g cm^{-3}]	1.711	+0.022, −0.048	E
$M_\star$ [M$_\odot$]	0.864	+0.084, −0.090	E
T magnitude	11.778	±0.018	G
Planetary parameters:			
a [AU]	0.0226	+0.0007, −0.0008	E
M_p [M$_{\rm Jup}$]	1.186	+0.090, −0.098	E
R_p [R$_{\rm Jup}$]	1.321	±0.039	E

NOTE— (A) From phase-folded TESS lightcurve (§ 2.2). Orbital periods are in Table 4. The limb darkening parameters were allowed to float around the Claret (2017) prediction, but were unconstrained. (B) Triaud et al. (2010). (C) From HARPS spectra (Doyle et al. 2013). (D) Stassun et al. (2017). (E) From functions of stellar, transit or RV parameters as discussed in text. (F) Gaia Collaboration et al. (2018). (G) Stassun et al. (2018).

ature, using the Stefan-Boltzmann law. To determine the stellar mass, we first computed the mean stellar density based on the value of $a/R_\star$ that gave the best fit to the phase-folded TESS lightcurve (for the relevant equation, see Seager & Mallén-Ornelas 2003 or Winn 2010). The mass was calculated from the radius and density, and the orbital distance was also calculated from the radius and $a/R_\star$. The planetary radius was calculated as the product of $R_\star$ and $R_{\rm p}/R_\star$. Finally, the planet mass was calculated based on the stellar mass, the radial-velocity amplitude observed by Triaud et al. (2010), and the orbital inclination.

Table 1 gives the resulting parameters, which we adopted for the remaining analysis. Our parameters are in agreement with those of previous investigators (Wilson et al. 2008; Gillon et al. 2009a; Winn et al. 2009; Southworth 2011; Petrucci et al. 2013). By comparing the star's luminosity and spectroscopic parameters with the outputs of the Yonsei-Yale stellar-evolutionary models, we found that WASP-4 is a main-sequence star with an age of approximately 7 Gyr.

3. TIMING ANALYSIS

3.1. *Pre-TESS timing measurements*

Table 2 gives the transit times we used in our analysis. We included data from peer-reviewed literature for which the analysis was based on observations of a single, complete transit, and for which the midpoint was allowed to be a free parameter. We also required that the time system be clearly
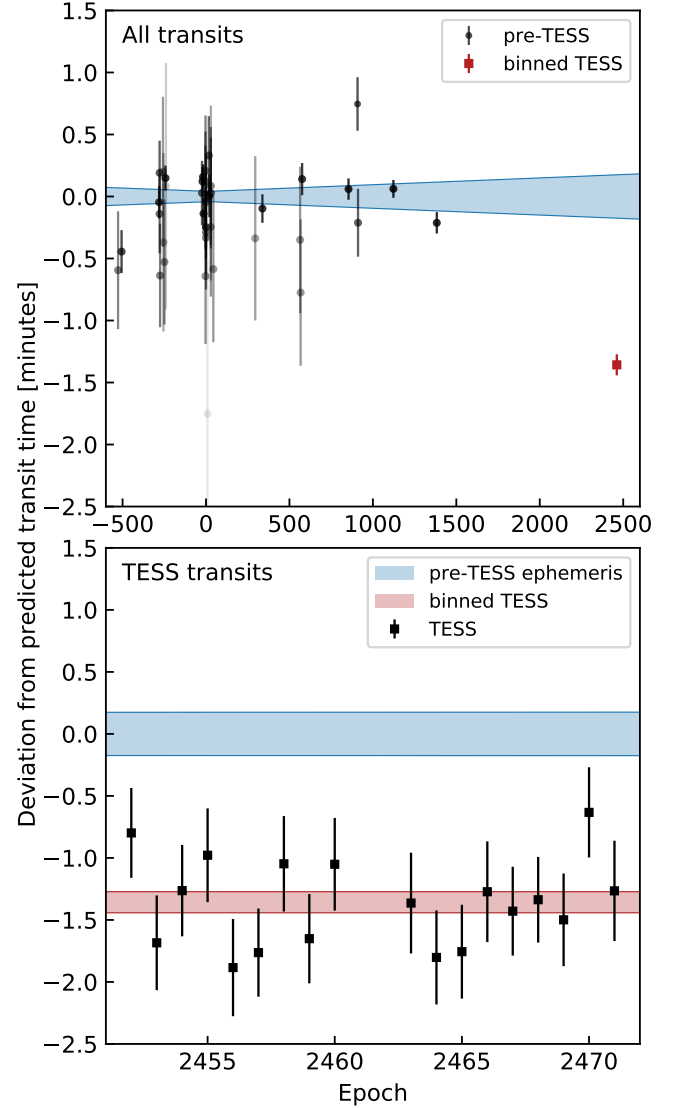

Figure 3. TESS saw WASP-4b transit earlier than expected. Both plots show the deviations between the observed and calculated transit times, where the calculation is based only on the pre-TESS data and assumes a constant period. The blue bands depict the $\pm 1\sigma$ credible interval of the predicted times. *Top:* The full timing dataset spans 11 years. The darkest points correspond to the most precise data. *Bottom:* Close-up of the TESS observations. The red band shows the average deviation of the TESS transits, which arrived 81.5 ± 11.7 seconds earlier than predicted.

documented. Many of the times were previously compiled by Hoyer et al. (2013). We confirmed that the times in that paper were in agreement with the original sources and that barycentric corrections had been performed when needed.

The earliest epoch is from EulerCam on the 1.2-m Euler telescope (Wilson et al. 2008). The second epoch is based on *z*-band photometry acquired by Gillon et al. (2009b) at the VLT 8.2-m with FORS2. Subsequent observations were performed by Winn et al. (2009), Dragomir et al. (2011),
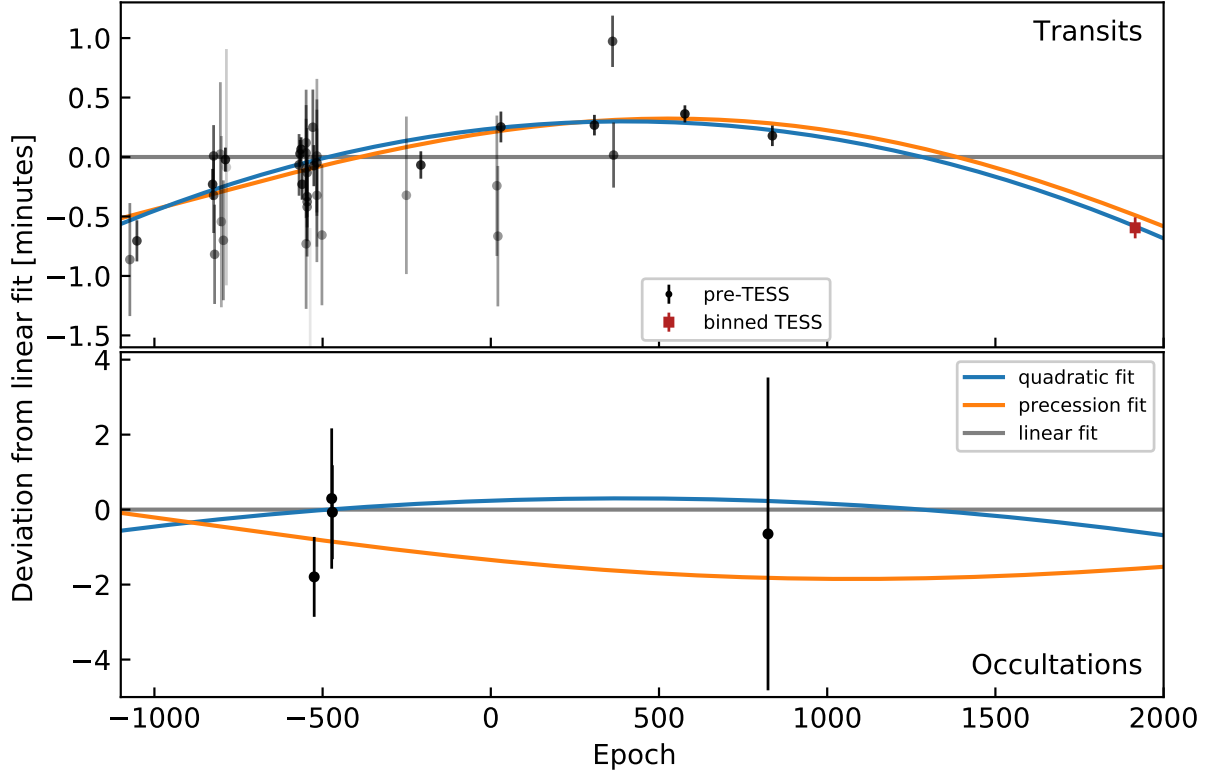
Figure 4. Timing residuals and best-fit models for WASP-4b. The residuals are the observed times minus the calculated times assuming a constant period. The darkest points correspond to the most precise data. The constant-period model (gray line) is a poor description of the data. Models with a uniformly decreasing period (blue) or apsidal precession (orange) provide better fits to the data. The red square represents the combination of all the TESS data and is for display purposes only. The models were fitted to all of the individual transit times.

Sanchis-Ojeda et al. (2011), Nikolov et al. (2012), Hoyer et al. (2013), and Ranjan et al. (2014). Finally, Huitson et al. (2017) acquired optical transit spectra with the 8.1-m Gemini South telescope between 2011 and 2014, one transit per season. The per-point standard deviation of their lightcurves was a few hundred parts per million. The average precision in their reported transit times was 5.6 seconds. Since those data points carry significant weight in the analysis, we consulted with those authors to confirm that the time stamps in their data represent mid-exposure times, that the barycentric correction was performed correctly, and that the time system of the final results was BJD$_{TDB}$. These same authors also used the same instrument (and largely the same software) to analyze other hot Jupiters, none of which showed a departure from a constant-period model.

We also compiled all the available occultation times, which are given in Table 3. The tabulated values have been corrected for the light-travel time across the diameter of the orbit by subtracting $2a/c = 22.8$ seconds from the observed time. Beerer et al. (2011) observed two occultations of WASP-4b using warm Spitzer in the 3.6 μm and 4.5 μm bands. Cáceres et al. (2011) detected an occultation from the ground in the K_S band, and gave a time in HJD, without specifying the time standard. We assumed the standard was UTC, and performed the appropriate corrections to convert to BJD$_{TDB}$. We also

verified that none of our conclusions would be changed if this assumption was mistaken. Finally, Zhou et al. (2015) observed an occultation with the Anglo-Australian Telescope. They did not report the observed midpoint, but they did report a result for $e\cos\omega$ based upon the observed midpoint. We calculated the implied midpoint using the formula (*e.g.*, Winn 2010)

$$t_{\rm occ}(E) = t_0 + PE + \frac{P}{2}\left(1 + \frac{4}{\pi}e\cos\omega\right). \qquad (1)$$

In total, there are four occultation times.

3.2. *Analysis*

First, we fitted a constant-period model ("linear ephemeris") to the pre-TESS data, and used it to extrapolate to the epochs of the TESS observations. The residuals of the best fitting model are shown in Figure 3. The transits observed by TESS occurred earlier than expected. Because the TESS mission is still in an early stage, we were concerned about a possible offset in the TESS time stamps due to an error with the TESS clock or the data processing pipeline. Appendix A describes some tests that convinced us that a simple offset is unlikely. Assuming that the observed timing variation is astrophysical, we proceeded by exploring three models for the timing data in a manner identical to the study by Patra et al. (2017).

The first model assumes a constant orbital period on a circular orbit:

$$t_{\text{tra}}(E) = t_0 + PE, \tag{2}$$

$$t_{\text{occ}}(E) = t_0 + \frac{P}{2} + PE, \tag{3}$$

where E is the epoch number. We defined the epoch numbers such that $E = 0$ is near the weighted average of the observed times. This helps to reduce the covariance between t_0 and P.

The second model assumes the period is changing at a steady rate:

$$t_{\text{tra}}(E) = t_0 + PE + \frac{1}{2}\frac{dP}{dE}E^2, \tag{4}$$

$$t_{\text{occ}}(E) = t_0 + \frac{P}{2} + PE + \frac{1}{2}\frac{dP}{dE}E^2. \tag{5}$$

The three free parameters are the reference epoch t_0, the period at the reference epoch, and the period derivative, $dP/dt = (1/P)dP/dE$.

The third model assumes the planet has a slightly eccentric orbit, and that the line of apsides is rotating (Giménez & Bastero 1995):

$$t_{\text{tra}}(E) = t_0 + P_{\text{s}}E - \frac{eP_{\text{a}}}{\pi}\cos\omega, \tag{6}$$

$$t_{\text{occ}}(E) = t_0 + \frac{P_{\text{a}}}{2} + P_{\text{s}}E + \frac{eP_{\text{a}}}{\pi}\cos\omega, \tag{7}$$

where P_{s} is the sidereal period, e is the eccentricity, P_{a} is the anomalistic period, and ω is the argument of pericenter. In this model the angular velocity of the line of apsides $d\omega/dE$ is constant,

$$\omega(E) = \omega_0 + \frac{d\omega}{dE}E, \tag{8}$$

and the sidereal and anomalistic periods are connected through the equation

$$P_{\text{s}} = P_{\text{a}}\left(1 - \frac{1}{2\pi}\frac{d\omega}{dE}\right). \tag{9}$$

The five free parameters of this model are $(t_0, P_{\text{s}}, e, \omega_0, d\omega/dE)$, denoting the reference epoch, the sidereal period, the eccentricity, the argument of pericenter at the reference epoch, and the angular velocity of the line of apsides.

Figure 4 shows the residuals with respect to the constant-period model. The best-fitting constant-period model has $\chi^2 = 174$ and 61 degrees of freedom. The best-fitting decreasing-period model has $\chi^2 = 62.6$ and 60 degrees of freedom. The best-fitting precession model has $\chi^2 = 64.4$ and 58 degrees of freedom. Either of the latter two models provides a much better fit than the constant-period model. The difference in χ^2 between the first and second models corresponds to $p \approx 10^{-26}$.

The decreasing-period model provides a slightly better fit to the data than the precession model. It is favored by $\Delta\chi^2 = 1.8$, and has two fewer free parameters. A useful heuristic for model comparison is the Bayesian Information Criterion (BIC),

$$\text{BIC} = \chi^2 + k\log n, \tag{10}$$

where k is the number of free parameters, and n is the number of data points. In this case, $n = 62$. The difference in the BIC between the precession and decay models is $\Delta\text{BIC} = \text{BIC}_{\text{prec}} - \text{BIC}_{\text{quad}} = 10$, corresponding to a Bayes factor of 1.2×10^4. Likewise, the Akaike Information Criterion favors the constant-period-derivative model by $\Delta\text{AIC} = 5.8$. Differences of this magnitude are traditionally deemed "strong evidence" that one model is a better description of the data than the other (Kass & Raftery 1995), although we prefer to reserve judgment until more data can be obtained.

In the decreasing-period model, the period derivative is

$$\dot{P} = -(3.98 \pm 0.38) \times 10^{-10} = -12.6 \pm 1.2\,\text{ms yr}^{-1}. \tag{11}$$

For comparison, the best-fitting period derivative of WASP-12b is $\dot{P} = -29 \pm 3\,\text{ms yr}^{-1}$ (Maciejewski et al. 2016; Patra et al. 2017). If both planets are truly falling onto their stars, then WASP-4b is falling at about half the rate of WASP-12b. In the precession model, the best-fit eccentricity is

$$e = (1.83^{+1.88}_{-0.75}) \times 10^{-3} \tag{12}$$

The longitude of periastron advances by $\dot{\omega} = 14.0^{+4.9}_{-3.5}$ degrees yr^{-1}, and the precession period is 26^{+9}_{-7} years. All of the best-fitting parameters (the medians of the posterior distributions) and the 68% credible intervals are reported in Table 4.

## 4. INTERPRETATION

4.1. *Orbital decay*

If the timing variation is being caused caused entirely by orbital decay, then the characteristic timescale of the decay is

$$\frac{P}{\dot{P}} = 9.2\,\text{Myr}. \tag{13}$$

For comparison, the corresponding time for WASP-12b is 3.2 Myr (Patra et al. 2017).

If WASP-4 really is undergoing rapid orbital decay, then how many of the other known hot Jupiters should have orbits that are decaying at detectable (or nearly detectable) rates? Figure 5 compares some key properties of WASP-4 with those of a larger ensemble of hot Jupiters. The middle panel displays two parameters that strongly affect the expected orbital decay timescale, $PM_\star/M_{\text{p}}$ and $a/R_\star$. WASP-4 has one of the shortest theoretical timescales for orbital decay. There are about 20 hot Jupiters (including WASP-12) for which the theoretical timescale is shorter. In almost all of those cases, though, the planet was discovered more recently than WASP-4 and a decade-long baseline of observations is not yet available. A separate consideration not shown in Figure 5 is that the hot Jupiter host stars have a variety of different structures, from being fully convective to nearly fully radiative, which may lead to widely divergent tidal dissipation timescales.

In the simple "constant phase lag" model for tidal interaction (Zahn 1977), the rate of dissipation can be parametrized
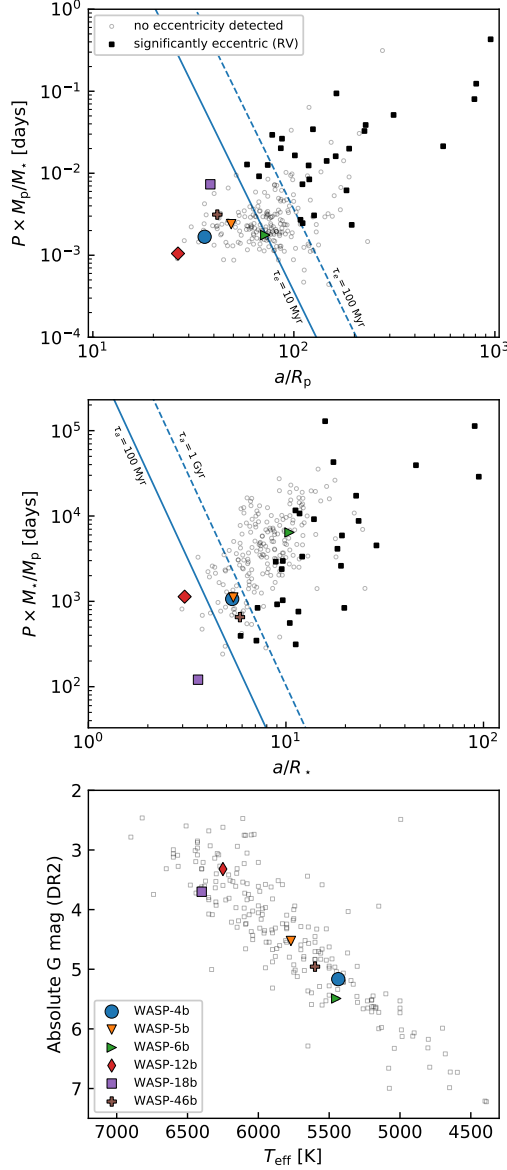
Figure 5. WASP-4b in the context of other hot Jupiters. Most of the data in these plots are from Bonomo et al. (2017), who measured the eccentricities using radial velocities. The colored symbols highlight WASP-4, WASP-12 (which also shows evidence for a decreasing period), and the collection of hot Jupiters analyzed in Appendix A. *Top:* The key parameters relevant to eccentricity damping. Solid squares represent planets with a securely detected nonzero eccentricity. Lines of constant damping timescale are drawn based on Equation 14 and assuming $Q'_p = 10^5$. WASP-4b has one of the shortest eccentricity damping timescales. *Middle:* Plotted are the key parameters relevant to orbital decay. Lines of constant decay timescale are drawn based on Equation 15, assuming $Q'_\star = 10^7$. WASP-4b has a relatively short orbital decay timescale, although it is not as extreme a case in this regard as it is for eccentricity damping. *Bottom:* A Hertzsprung-Russell diagram for hot Jupiter hosts. WASP-4 appears to be on the main sequence.

by a modified[3] quality factor, $Q'_\star = 3Q_\star/(2k_\star)$. Here, $Q_\star$ is the ratio between the energy stored in the equilibrium deformation of the star and the energy lost to heat per tidal period (*e.g.*, Goldreich & Soter 1966). A larger $Q_\star$ implies less efficient tidal dissipation. The dimensionless number $k_\star$ is the stellar Love number, which is smaller when the star's density distribution is more centrally concentrated. In this model, once the planet's spin and orbit are synchronized, then the semi-major axis and eccentricity evolve as (Appendix B of Metzger et al. 2012)

$$\frac{1}{\tau_e} = \frac{|\dot{e}|}{e} = \frac{63\pi}{2Q'_p} \left(\frac{R_p}{a}\right)^5 \left(\frac{M_\star}{M_p}\right) \left(\frac{1}{P}\right) \quad (14)$$

$$\frac{1}{\tau_a} = \frac{|\dot{a}|}{a} = \frac{9\pi}{Q'_\star} \left(\frac{R_\star}{a}\right)^5 \left(\frac{M_p}{M_\star}\right) \left(\frac{1}{P}\right). \quad (15)$$

The orbital period evolves as

$$\dot{P} = -\frac{27\pi}{2Q'_\star} \left(\frac{M_p}{M_\star}\right) \left(\frac{R_\star}{a}\right)^5. \quad (16)$$

The modified quality factor of WASP-4 corresponding to the observed value of $\dot{P}$ is

$$Q'_\star \approx 2.9 \times 10^4. \quad (17)$$

This is about an order of magnitude lower than the value that was inferred for WASP-12b. It is also smaller than most theoreticians would have expected. The Q'_{Jup} value of Jupiter is estimated to be $\approx 1.4 \times 10^5$, based on the observed motions of the Galilean moons (Lainey et al. 2009). For stars, studies of the binary eccentricity distribution have been interpreted with tidal models, giving $Q'_\star \approx 10^5 - 10^7$ (*e.g.*, Meibom & Mathieu 2005; Belczynski et al. 2008; Geller et al. 2013; Milliman et al. 2014). Population studies of hot Jupiter systems have also been undertaken, generally finding $Q'_\star \approx 10^5 - 10^8$ using different models (Jackson et al. 2009; Hansen 2010; Penev et al. 2012, 2018; Collier Cameron & Jardine 2018). For instance, motivated by the rapid rotation of some hot Jupiter hosts (Pont 2009; Ciceri et al. 2016a; Penev et al. 2016), Penev et al. (2018) modeled the evolution of hot Jupiter systems under the influence of a magnetized wind and a constant phase-lag tide. For WASP-4, their method gave $Q'_\star \approx (1.2^{+1.0}_{-0.5}) \times 10^7$. This strongly disagrees with the quality factor we have inferred from the apparent period change.

Essick & Weinberg (2016) studied the problem of the orbital decay of hot Jupiters using a theory in which gravity modes are excited at the base of the stellar convective zone, propagate inward through the radiative core and break near the stellar core, leading to energy dissipation. They predicted the stellar quality factors in hot Jupiter systems to vary from $Q'_\star \approx 10^5 - 10^6$. From their Equation 26, the prediction for

---

[3] For stars, $k_\star \sim \mathcal{O}(10^{-2})$, so it is important to explicitly distinguish $Q'_\star$ from $Q_\star$ (*e.g.*, Schwarzschild 1958).

WASP-4 is $Q'_\star = 7 \times 10^5$, which is an order of of magnitude larger than implied by the observed period change.

The applicability of the Essick & Weinberg (2016) model depends on the evolutionary state of the star. Weinberg et al. (2017) showed that more rapid dissipation — enough to account for the period change of WASP-12b — could exist in stars that have begun evolving into red giants. The bottom panel of Figure 5 shows a Hertzsprung-Russell diagram of hot Jupiters hosts, including WASP-4. On the y-axis is $G = g - \mu$, for g the apparent Gaia-band magnitude, and μ the distance modulus reported by Gaia Collaboration et al. (2018). The x-axis is the effective temperature from Bonomo et al. (2017), which for WASP-4 agrees within 1σ of that from Table 1. Inspecting the HR diagram, WASP-4 shows little evidence of being evolved, in agreement with our analysis from § 2.3.

To summarize, if the observed period change is caused entirely by tidal orbital decay, then the constant-phase-lag tidal model implies a stellar tidal dissipation rate that is higher than expected by at least an order of magnitude. It might be possible that we are observing at a special time, shortly after the planet's inward migration, or when the planet is near resonance with a stellar oscillation mode. Tidal dissipation rates might also be increased if the star is just turning off the main sequence. Another hypothesis, recently advanced by Millholland & Laughlin (2018) for the case of WASP-12b, is that an exterior planet could be trapping WASP-4b's spin vector in a high-obliquity state, leading to rapid dissipation through planetary obliquity tides.

4.2. Apsidal precession

If instead the observed timing variation is just a small portion of an apsidal precession cycle, then the orbital eccentricity is a few times 10^{-3}, and the full precession period is about 24 years. Ragozzine & Wolf (2009) calculated apsidal precession periods for hot Jupiters, finding them to range between about 10 and 100 years. They highlighted that for many hot Jupiters, including WASP-4b, the theoretical precession rate is dominated by the non-Keplerian force due to the planet's tidal bulge. Precession from general relativity, the planet's rotational bulge, and the star's rotational and tidal bulges contribute at the 10% level at most. Thus, a measurement of the precession rate can be used to determine the planet's Love number. From their Equation 14, the implied Love number for WASP-4b is

$$k_{2,p} = 1.5^{+2.1}_{-1.1}. \tag{18}$$

For comparison, the Love number of Jupiter is about 0.55 (Wahl et al. 2016; Ni 2018), and a uniform density sphere has $k_2 = 1.5$. The uncertainty in $k_{2,p}$ for WASP-4b is large because the eccentricity, reference time, and $d\omega/dE$ have strongly correlated errors, and the measured occultation times only barely constrain these parameters (Figure 6).

The main problem with the apsidal precession hypothesis is to explain why the eccentricity would be as large as $\sim 10^{-3}$ despite rapid tidal circularization. For WASP-4, Equation 14

gives $\tau_e = 0.30(Q'_p/10^5)$ Myr. The star is several billion years old, so unless the planet arrived very recently, any initial eccentricity should have been lowered well below $\sim 10^{-3}$. The top panel of Figure 5 compares the expected eccentricity damping time of WASP-4b with that of other transiting giant planets. WASP-4b has one of the shortest known eccentricity damping times.

Neighboring companion — One way to maintain a significant eccentricity is through the gravitational perturbations from another planet. Mardling (2007) considered the long-term tidal evolution of hot Jupiters with companions. The companion in their model is coplanar, and can have a mass down to an Earth-mass; the main requirement is that both the hot Jupiter and the outer companion start on eccentric orbits. They found that although the early phases of the two-planet eccentricity evolution occur quickly, the final phase of the joint eccentricity evolution towards circularity would occur on timescales several orders of magnitude longer than the circularization time of an isolated hot Jupiter (see their Figures 4 and 5).

A different way to excite the hot Jupiter's eccentricity is the Kozai-Lidov mechanism (Lidov 1962; Kozai 1962). In this case, the orbital plane of the outer companion, "c", would need to be inclined relative to that of the hot Jupiter, "b", by at least $\sin^{-1}\sqrt{2/5} \approx 39°$. For the Kozai-Lidov mechanism to operate at maximum efficiency, we need (Bailey & Goodman 2019, Equation 20)

$$M_c > 7.1\, M_\oplus \times \left(\frac{a_c}{a_b}\right)^{3/2}, \tag{19}$$

where $M_{b,c}$ and $a_{b,c}$ are the mass and semi-major axis of WASP-4b and the hypothetical WASP-4c, and we have assumed WASP-4b's Love number is $k_{2,b} \approx 0.6$. For the RV signal of the companion to remain undetected, it would need to be in the residual $(O-C)_{RV} = 15.2\,\text{ms}^{-1}$ reported by Triaud et al. (2010). Again following Bailey & Goodman (2019), this implies

$$M_c < (O-C)_{RV} \left(\frac{M_\star a_b}{G}\right)^{1/2} \left(\frac{a_c}{a_b}\right)^{1/2} f^{-1/2}$$
$$M_c < 23.8\, M_\oplus \times \left(\frac{a_c}{a_b}\right)^{1/2} f^{-1/2}, \tag{20}$$

for $f(e_c, \omega_c, i_c) \propto \sin^2 i_c$ a geometric prefactor that depends on the argument of periastron ω_c and inclination i_c of the exterior companion (Bailey & Goodman 2019 Equation 23). Since WASP-4b is transiting, f can be arbitrarily small, and both of the preceding limits can be satisfied.

Fluctuations in the gravitational potential from convection — A separate mechanism to pump the eccentricity invokes the gravitational fluctuations from stellar convection (Phinney 1992, Section 7). From equation 7.33 of that work, the mean-squared eccentricity of the orbit is

$$\langle e^2 \rangle = \frac{2\langle E_e \rangle}{\mu n^2 a^2} = 6.8 \times 10^{-5} \frac{(L^2 R_{conv}^2 M_{conv}^2)^{1/3}}{\mu n^2 a^2}, \tag{21}$$

where L is the stellar luminosity, R_{conv} and M_{conv} are the width and mass of the convective region, μ is the reduced mass, n is the orbital frequency, and a is the semi-major axis. For WASP-4, this equation implies $\langle e^2 \rangle^{1/2} \lesssim 10^{-5}$. Hence, this mechanism does not seem capable of producing the required value of $\sim 10^{-3}$.

4.3. *Applegate effect*

Some eclipsing binaries exhibit period modulations with amplitudes of $\lesssim 0.05$ days over timescales of decades (*e.g.*, Söderhjelm 1980; Hall 1989). Applegate (1992) proposed a mechanism to explain these modulations in which the internal structure of a magnetically active star changes shape via cyclic exchange of angular momentum between the inner and outer zones of the star. This model could also apply to a hot Jupiter orbiting a star with a convective zone. The changing gravitational quadrupole of the star would cause the orbit of the planet to precess on the timescale of the stellar activity cycle. An essential difference between this process and apsidal precession is that Applegate timing variations need not be strictly periodic (*e.g.*, Söderhjelm 1980, Figure 12). This mechanism would also produce transit and occultation timing deviations of the same sign, while for apsidal precession they would have opposite signs. For WASP-4, Watson & Marsh (2010) estimated that the Applegate effect could produce timing deviations of up to 15 seconds, depending on the modulation period of the stellar dynamo, and the corresponding level of differential surface shear. If this analysis is accurate, then the Applegate mechanism cannot explain the majority our observed 82 second variation.

4.4. *Other possible explanations*

An apparent change in orbital period can also be caused by an overall acceleration of the center of mass of the system. This would produce a period derivative

$$\dot{P} \approx \frac{\dot{v}_r P}{c}, \tag{22}$$

where $\dot{v}_r$ is the time derivative of the radial velocity. Knutson et al. (2014) combined radial-velocity data from their own program as well as those of Wilson et al. (2008), Pont et al. (2011), and Husnoo et al. (2012) to obtain a constraint on any long-term trend:

$$\dot{v}_r = -0.0099^{+0.0052}_{-0.0054}\,\mathrm{m\,s^{-1}\,day^{-1}}, \tag{23}$$

which can also be expressed as a 2σ upper limit of $0.021\,\mathrm{m\,s^{-1}\,day^{-1}}$ on the acceleration along the line of sight. The associated upper limit on the apparent period change resulting from this acceleration is 9×10^{-11}, which is only one-quarter of the observed period decrease (Equation 11).

Thus, it seems that the observed period decrease cannot be fully explained as a constant acceleration of the center of mass of WASP-4. Given the limited amount and uneven time coverage of the existing radial-velocity data, it remains possible that the center of mass has a more complex motion, due to a companion on a highly eccentric orbit (similar to
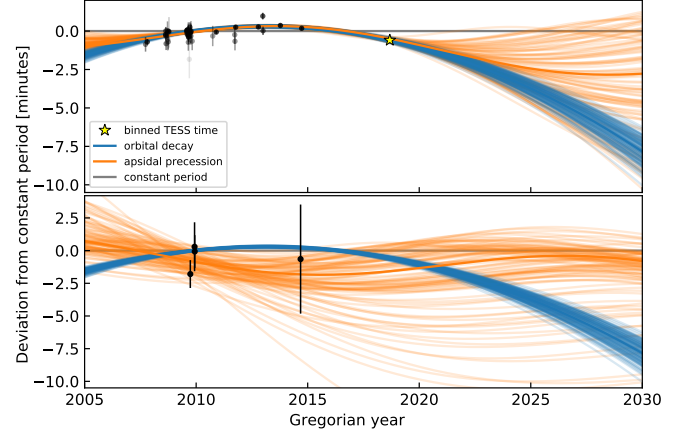
Figure 6. Further observations will be needed to confirm and understand the timing variations of WASP-4b. Dots are as in Figure 4. Lines are 100 random draws from the posteriors of the apsidal precession model (orange), and the orbital decay model (blue).

e.g., WASP-53 or WASP-81 Triaud et al. 2017). It would be useful to gather more radial-velocity data to confirm or refute this possibility.

There are two other small effects worth noting. The first is the Shklovskii (1970) effect due to the star's proper motion, which leads to an apparent period change of $P\mu^2 d/c$, which is only 6×10^{-13} for the case of WASP-4. The second effect, described by Rafikov (2009), comes from the star's on-sky motion altering our viewing angle, and leads to an observed apsidal precession. The corresponding period change is $\dot{P} \sim (P\mu)^2/2\pi$, which is on the order of 10^{-21} for WASP-4, too small to be of any consequence.

5. CALL FOR ADDITIONAL OBSERVATIONS

A primary purpose of this work has been to call attention to the timing anomaly of WASP-4 that has been sighted by TESS, and alert observers to the need for follow-up transit timing, occultation timing, and radial-velocity monitoring. There is no unique interpretation of the current data, and two of the possibilities — orbital decay and apsidal precession — would be of great interest to confirm. Detection of orbital decay would lead to an unusually direct determination of a stellar dissipation rate. Detection of apsidal precession would give a rare constraint on the interior density distribution of an exoplanet.

If the TESS mission is extended after its primary mission, it will likely observe additional transits of WASP-4b in the early 2020s (Figure 6). High-precision transit observations with larger telescopes would also be useful. In order to decide between orbital decay and apsidal precession, occultation measurements in both the near term and also in the mid-2020s will be needed. More radial-velocity data would help in the search for additional bodies that could be causing dynamical perturbations, or an overall acceleration of the host star.

TESS will also be monitoring the other known hot Jupiters, which will reveal whether the timing anomalies seen in WASP-12 and now WASP-4 are commonplace, and may shed some light on the circumstances in which they arise. Other wide-field photometric surveys, such as the Next Generation Transit Survey (Wheatley et al. 2018), HATPI (hatpi.org) and PLATO (Rauer et al. 2014) will also extend the time baseline of transit timing for a large number of systems.

Facility: TESS (Ricker et al. 2015), Gaia (Gaia Collaboration et al. 2016, 2018)

Software: astrobase (Bhatti et al. 2018), astropy (Collaboration et al. 2018), astroquery (Ginsburg et al. 2018), BATMAN (Kreidberg 2015), corner (Foreman-Mackey 2016), emcee (Foreman-Mackey et al. 2013), IPython (Pérez & Granger 2007), matplotlib (Hunter 2007), numpy (Walt et al. 2011), pandas (McKinney 2010), scikit-learn (Pedregosa et al. 2011), scipy (Jones et al. 2001).

Table 2. WASP-4b transit times, uncertainties, and references.

t_{tra} [BJD$_{TDB}$]	$\sigma_{t_{tra}}$ [days]	Epoch	H13?	Reference
2454368.59279	0.00033	-1073	1	Wilson et al. (2008)
2454396.69576	0.00012	-1052	1	Gillon et al. (2009b)
2454697.79817	0.00009	-827	1	Winn et al. (2009)
2454701.81303	0.00018	-824	1	Hoyer et al. (2013)
2454701.81280	0.00022	-824	1	Hoyer et al. (2013)
2454705.82715	0.00029	-821	1	Hoyer et al. (2013)
2454728.57767	0.00042	-804	1	Hoyer et al. (2013)
2454732.59197	0.00050	-801	1	Hoyer et al. (2013)
2454740.62125	0.00035	-795	1	Hoyer et al. (2013)
2454748.65111	0.00007	-789	1	Winn et al. (2009)
2454752.66576	0.00069	-786	1	Dragomir et al. (2011)
2455041.72377	0.00018	-570	1	Hoyer et al. (2013)
2455045.73853	0.00008	-567	1	Sanchis-Ojeda et al. (2011)
2455049.75325	0.00007	-564	1	Sanchis-Ojeda et al. (2011)
2455053.76774	0.00009	-561	1	Sanchis-Ojeda et al. (2011)
2455069.82661	0.00029	-549	1	Nikolov et al. (2012)
2455069.82617	0.00038	-549	1	Nikolov et al. (2012)
2455069.82670	0.00028	-549	1	Nikolov et al. (2012)
2455069.82676	0.00031	-549	1	Nikolov et al. (2012)
2455073.84108	0.00029	-546	1	Nikolov et al. (2012)
2455073.84128	0.00026	-546	1	Nikolov et al. (2012)
2455073.84111	0.00023	-546	1	Nikolov et al. (2012)
2455073.84114	0.00018	-546	1	Nikolov et al. (2012)
2455085.88418	0.00086	-537	1	Dragomir et al. (2011)
2455096.59148	0.00022	-529	1	Hoyer et al. (2013)
2455100.60595	0.00012	-526	1	Sanchis-Ojeda et al. (2011)
2455112.64986	0.00039	-517	1	Nikolov et al. (2012)
2455112.65009	0.00033	-517	1	Nikolov et al. (2012)
2455112.65005	0.00031	-517	1	Nikolov et al. (2012)
2455112.65005	0.00049	-517	1	Nikolov et al. (2012)
2455132.72310	0.00041	-502	1	Hoyer et al. (2013)
2455468.61943	0.00046	-251	1	Hoyer et al. (2013)
2455526.16356	0.00008	-208	0	Ranjan et al. (2014)
2455828.60375	0.00041	18	1	Hoyer et al. (2013)
2455832.61815	0.00041	21	1	Hoyer et al. (2013)
2455844.66287	0.00009	30	0	Huitson et al. (2017)
2456216.69123	0.00006	308	0	Huitson et al. (2017)
2456288.95622	0.00015	362	0	Baxter et al. (in prep)
2456292.97025	0.00019	365	0	Baxter et al. (in prep)
2456576.67556	0.00005	577	0	Huitson et al. (2017)
2456924.61561	0.00006	837	0	Huitson et al. (2017)
2458355.18490	0.00025	1906	0	This work
2458356.52251	0.00027	1907	0	This work
2458357.86104	0.00026	1908	0	This work
2458359.19947	0.00026	1909	0	This work
2458360.53707	0.00027	1910	0	This work
2458361.87539	0.00025	1911	0	This work
2458363.21411	0.00027	1912	0	This work
2458364.55193	0.00025	1913	0	This work
2458365.89058	0.00026	1914	0	This work
2458369.90505	0.00028	1917	0	This work
2458371.24298	0.00026	1918	0	This work
2458372.58124	0.00026	1919	0	This work
2458373.91981	0.00028	1920	0	This work

Table 2 continued

Table 2 *(continued)*

$t_{\rm tra}$ [BJD$_{\rm TDB}$]	$\sigma_{t_{\rm tra}}$ [days]	Epoch	H13?	Reference
2458375.25793	0.00025	1921	0	This work
2458376.59623	0.00024	1922	0	This work
2458377.93435	0.00026	1923	0	This work
2458379.27318	0.00025	1924	0	This work
2458380.61098	0.00028	1925	0	This work

NOTE— $t_{\rm tra}$ is the measured transit midtime, and $\sigma_{t_{\rm tra}}$ is its 1σ uncertainty. σ_{t_0} was evaluated from the sampled posteriors by taking the maximum of the difference between the 84th percentile minus the median, and the median minus the 16th percentile. The "Reference" column refers to the work describing the original observations. The "H13?" column is 1 if the mid-time value was taken from Hoyer et al. (2013). Otherwise, the mid-time came from the column listed in "Reference". The Hoyer et al. (2013) BJD$_{\rm TT}$ times are equal to BJD$_{\rm TDB}$ for our purposes (Urban & Seidelmann 2012). We omitted the timing measurements from Southworth et al. (2009), since there were technical problems with the computer clock at the time of observation (Nikolov et al. 2012). The two Baxter et al. (in prep) times were obtained from Spitzer/IRAC transit light curves in the $3.6\,\mu$m and $4.5\,\mu$m channels.

Table 3. WASP-4b occultation times, uncertainties, and references.

$t_{\rm occ}$ [BJD$_{\rm TDB}$]	$\sigma_{t_{\rm occ}}$ [days]	Epoch	Reference
2455102.61210	0.00074	-511	Cáceres et al. (2011)[a]
2455172.20159	0.00130	-459	Beerer et al. (2011)
2455174.87780	0.00087	-457	Beerer et al. (2011)
2456907.88714	0.00290	838	Zhou et al. (2015)[b]

NOTE— $t_{\rm occ}$ is the measured occultation midtime, minus the $2a/c = 22.8$ second light travel time; $\sigma_{t_{\rm occ}}$ is the 1σ uncertainty on the occultation time.

[a] Cáceres et al. (2011) reported this time in "HJD", with an unspecified time standard. We assumed the time was originally in HJD$_{\rm UTC}$, and converted to BJD$_{\rm TDB}$ for the tabulated time.

[b] Zhou et al. (2015) fixed the epoch, and let $e\cos\omega$ float. Using the reported dates of observation, we converted their $e\cos\omega$ values into an occultation time using Equation 1 of the text.

Table 4. Best-fit model parameters.

Parameter	Median Value (Unc.)[a]
Constant period	
t_0 [BJD$_{\rm TBD}$]	2455804.515751(+19)(-19)
P [days]	1.338231466(+23)(-23)
Constant period derivative	
t_0 [BJD$_{\rm TBD}$]	2455804.515917(+25)(-24)
P [days]	1.338231678(+30)(-31)
dP/dt	$-3.98(+38)(-38)\times 10^{-10}$
Apsidal precession	
t_0 [BJD$_{\rm TBD}$]	2455804.51531(+25)(-30)
$P_{\rm s}$ [days]	1.33823130(+18)(-41)
e	$1.83^{+1.58}_{-0.75}\times 10^{-3}$

Table 4 continued

Table 4 *(continued)*

Parameter	Median Value (Unc.)[a]
ω_0 [rad]	2.42(+38)(-32)
$d\omega/dE$ [rad epoch^{-1}]	$8.94^{+3.16}_{-2.23}\times 10^{-4}$

[a] The numbers in parenthesis give the 68% confidence interval for the final two digits, where appropriate.

REFERENCES

Anderson, D. R., Gillon, M., Hellier, C., et al. 2008, Monthly Notices of the Royal Astronomical Society, 387, L4

Anderson, D. R., Collier Cameron, A., Gillon, M., et al. 2012, Monthly Notices of the Royal Astronomical Society, 422, 1988

Applegate, J. H. 1992, The Astrophysical Journal, 385, 621

Bailey, A., & Goodman, J. 2019, Monthly Notices of the Royal Astronomical Society, 482, 1872

Beerer, I. M., Knutson, H. A., Burrows, A., et al. 2011, The Astrophysical Journal, 727, 23

Belczynski, K., Kalogera, V., Rasio, F. A., et al. 2008, The Astrophysical Journal Supplement Series, 174, 223

Bhatti, W., Bouma, L. G., & Wallace, J. 2018, astrobase

Bonomo, A. S., Desidera, S., Benatti, S., et al. 2017, Astronomy and Astrophysics, 602, A107

Borkovits, T., Rappaport, S., Hajdu, T., & Sztakovics, J. 2015, Monthly Notices of the Royal Astronomical Society, 448, 946

Cáceres, C., Ivanov, V. D., Minniti, D., et al. 2011, Astronomy and Astrophysics, 530, A5

Ciceri, S., Mancini, L., Henning, T., et al. 2016a, Publications of the Astronomical Society of the Pacific, 128, 074401

Ciceri, S., Mancini, L., Southworth, J., et al. 2016b, Monthly Notices of the Royal Astronomical Society, 456, 990

Claret, A. 2017, Astronomy & Astrophysics, 600, A30, arXiv: 1804.10295

Collaboration, T. A., Price-Whelan, A. M., Sipöcz, B. M., et al. 2018, arXiv:1801.02634 [astro-ph], arXiv: 1801.02634

Collier Cameron, A., & Jardine, M. 2018, Monthly Notices of the Royal Astronomical Society, 476, 2542

Counselman, C. C. 1973, The Astrophysical Journal, 180, 307

Doyle, A. P., Smalley, B., Maxted, P. F. L., et al. 2013, Monthly Notices of the Royal Astronomical Society, 428, 3164

Dragomir, D., Kane, S. R., Pilyavsky, G., et al. 2011, The Astronomical Journal, 142, 115

Eastman, J., Siverd, R., & Gaudi, B. S. 2010, Publications of the Astronomical Society of the Pacific, 122, 935, arXiv: 1005.4415

Essick, R., & Weinberg, N. N. 2016, The Astrophysical Journal, 816, 18

Foreman-Mackey, D. 2016, The Journal of Open Source Software, 24

Foreman-Mackey, D., Hogg, D. W., Lang, D., & Goodman, J. 2013, Publications of the Astronomical Society of the Pacific, 125, 306

Fukui, A., Narita, N., Tristram, P. J., et al. 2011, Publications of the Astronomical Society of Japan, 63, 287

Gaia Collaboration, Prusti, T., de Bruijne, J. H. J., et al. 2016, Astronomy and Astrophysics, 595, A1

Gaia Collaboration, Brown, A. G. A., Vallenari, A., et al. 2018, Astronomy and Astrophysics, 616, A1

Geller, A. M., Hurley, J. R., & Mathieu, R. D. 2013, The Astronomical Journal, 145, 8

Gillon, M., Anderson, D. R., Triaud, A. H. M. J., et al. 2009a, Astronomy and Astrophysics, 501, 785

Gillon, M., Smalley, B., Hebb, L., et al. 2009b, Astronomy and Astrophysics, 496, 259

Giménez, A., & Bastero, M. 1995, Astrophysics and Space Science, 226, 99

Ginsburg, A., Sipocz, B., Madhura Parikh, et al. 2018, Astropy/Astroquery: V0.3.7 Release

Goldreich, P., & Soter, S. 1966, Icarus, 5, 375

Goodman, J., & Weare, J. 2010, Communications in Applied Mathematics and Computational Science, 5, 65

Hall, D. S. 1989, Space Science Reviews, 50, 219

Hansen, B. M. S. 2010, The Astrophysical Journal, 723, 285

Hellier, C., Anderson, D. R., Collier Cameron, A., et al. 2009, Nature, 460, 1098

Hoyer, S., Rojo, P., & López-Morales, M. 2012, The Astrophysical Journal, 748, 22

Hoyer, S., López-Morales, M., Rojo, P., et al. 2013, Monthly Notices of the Royal Astronomical Society, 434, 46

Huitson, C. M., Désert, J.-M., Bean, J. L., et al. 2017, The Astronomical Journal, 154, 95

Hunter, J. D. 2007, Computing in Science & Engineering, 9, 90

Husnoo, N., Pont, F., Mazeh, T., et al. 2012, Monthly Notices of the Royal Astronomical Society, 422, 3151

Hut, P. 1980, Astronomy and Astrophysics, 92, 167

Jackson, B., Barnes, R., & Greenberg, R. 2009, The Astrophysical Journal, 698, 1357

Jenkins, J. M., Twicken, J. D., McCauliff, S., et al. 2016, Software and Cyberinfrastructure for Astronomy IV, 9913, 99133E

Jones, E., Oliphant, T., Peterson, P., et al. 2001, Open source scientific tools for Python

Jordán, A., Espinoza, N., Rabus, M., et al. 2013, The Astrophysical Journal, 778, 184

Kass, R. E., & Raftery, A. E. 1995, Journal of the American Statistical Association, 90, 773

Knutson, H. A., Fulton, B. J., Montet, B. T., et al. 2014, The Astrophysical Journal, 785, 126

Kostov, V. B., McCullough, P. R., Carter, J. A., et al. 2014, The Astrophysical Journal, 784, 14

Kovács, G., Zucker, S., & Mazeh, T. 2002, Astronomy and Astrophysics, 391, 369

Kozai, Y. 1962, The Astronomical Journal, 67, 591

Kreidberg, L. 2015, Publications of the Astronomical Society of the Pacific, 127, 1161

Lainey, V., Arlot, J.-E., Karatekin, Ã., & van Hoolst, T. 2009, Nature, 459, 957

Levrard, B., Winisdoerffer, C., & Chabrier, G. 2009, The Astrophysical Journal, 692, L9

Lidov, M. L. 1962, Planetary and Space Science, 9, 719

Maciejewski, G., Dimitrov, D., FernÃ¡ndez, M., et al. 2016, Astronomy and Astrophysics, 588, L6

Mandel, K., & Agol, E. 2002, The Astrophysical Journal, 580, L171, arXiv: astro-ph/0210099

Mansouri-Samani, M., et al. 2018, TESS Science Data Products Description Document, EXP-TESS-ARC-ICD-0014, https://archive.stsci.edu/missions/tess/doc/ EXP-TESS-ARC-ICD-TM-0014.pdf

Mardling, R. A. 2007, Monthly Notices of the Royal Astronomical Society, 382, 1768

Masuda, K. 2015, The Astrophysical Journal, 805, 28

—. 2017, The Astronomical Journal, 154, 64

Matsumura, S., Peale, S. J., & Rasio, F. A. 2010, The Astrophysical Journal, 725, 1995

Maxted, P. F. L., Anderson, D. R., Doyle, A. P., et al. 2013, Monthly Notices of the Royal Astronomical Society, 428, 2645

Mazeh, T. 2008, in EAS Publications Series, Vol. 29, EAS Publications Series, ed. M.-J. Goupil & J.-P. Zahn, 1

McKinney, W. 2010, in Proceedings of the 9th Python in Science Conference, ed. S. van der Walt & J. Millman, 51

Meibom, S., & Mathieu, R. D. 2005, The Astrophysical Journal, 620, 970

Metzger, B. D., Giannios, D., & Spiegel, D. S. 2012, Monthly Notices of the Royal Astronomical Society, 425, 2778

Millholland, S., & Laughlin, G. 2018, arXiv:1812.01624 [astro-ph], arXiv: 1812.01624

Milliman, K. E., Mathieu, R. D., Geller, A. M., et al. 2014, The Astronomical Journal, 148, 38

Mills, S. M., & Fabrycky, D. C. 2017, The Astronomical Journal, 153, 45

Moyano, M., Almeida, L. A., von Essen, C., Jablonski, F., & Pereira, M. G. 2017, Monthly Notices of the Royal Astronomical Society, 471, 650

Ni, D. 2018, Astronomy & Astrophysics, 613, A32

Nikolov, N., Henning, T., Koppenhoefer, J., et al. 2012, Astronomy and Astrophysics, 539, A159

Nikolov, N., Sing, D. K., Burrows, A. S., et al. 2015, Monthly Notices of the Royal Astronomical Society, 447, 463

Ogilvie, G. I. 2014, Annual Review of Astronomy and Astrophysics, 52, 171, arXiv: 1406.2207

Patra, K. C., Winn, J. N., Holman, M. J., et al. 2017, The Astronomical Journal, 154, 4

Pedregosa, F., Varoquaux, G., Gramfort, A., et al. 2011, Journal of Machine Learning Research, 12, 2825

Penev, K., Bouma, L. G., Winn, J. N., & Hartman, J. D. 2018, The Astronomical Journal, 155, 165

Penev, K., Jackson, B., Spada, F., & Thom, N. 2012, The Astrophysical Journal, 751, 96

Penev, K., Hartman, J. D., Bakos, G. Ã., et al. 2016, The Astronomical Journal, 152, 127

Pérez, F., & Granger, B. E. 2007, Computing in Science and Engineering, 9, 21

Petrucci, R., Jofré, E., Ferrero, L. V., et al. 2018, Monthly Notices of the Royal Astronomical Society, 473, 5126

Petrucci, R., Jofré, E., Schwartz, M., et al. 2013, The Astrophysical Journal Letters, 779, L23

Phinney, E. S. 1992, Philosophical Transactions of the Royal Society of London Series A, 341, 39

Pont, F. 2009, Monthly Notices of the Royal Astronomical Society, 396, 1789

Pont, F., Husnoo, N., Mazeh, T., & Fabrycky, D. 2011, Monthly Notices of the Royal Astronomical Society, 414, 1278

Rafikov, R. R. 2009, The Astrophysical Journal, 700, 965

Ragozzine, D., & Wolf, A. S. 2009, The Astrophysical Journal, 698, 1778, arXiv: 0807.2856

Ranjan, S., Charbonneau, D., Désert, J.-M., et al. 2014, The Astrophysical Journal, 785, 148

Rauer, H., Catala, C., Aerts, C., et al. 2014, Experimental Astronomy, 38, 249

Ricker, G., & Vanderspek, R. 2018, Data Products From TESS Data Alerts, https://archive.stsci.edu/prepds/tess-data-alerts/index.html

Ricker, G. R., Winn, J. N., Vanderspek, R., et al. 2015, Journal of Astronomical Telescopes, Instruments, and Systems, 1, 014003

Sada, P. V., Deming, D., Jennings, D. E., et al. 2012, Publications of the Astronomical Society of the Pacific, 124, 212

Sanchis-Ojeda, R., Winn, J. N., Holman, M. J., et al. 2011, The Astrophysical Journal, 733, 127

Schwarzschild, M. 1958, Structure and evolution of the stars (Princeton Univesity Press), Ch. 18

Seager, S., & Mallén-Ornelas, G. 2003, The Astrophysical Journal, 585, 1038

Shklovskii, I. S. 1970, Soviet Astronomy, 13, 562

Smith, J. C., Morris, R. L., Jenkins, J. M., et al. 2017a, Kepler Science Document, 7

Smith, J. C., Stumpe, M. C., Jenkins, J. M., et al. 2017b, Kepler Science Document, 8

Söderhjelm, S. 1980, Astronomy and Astrophysics, 89, 100

Southworth, J. 2011, Monthly Notices of the Royal Astronomical Society, 417, 2166

Southworth, J., Hinse, T. C., Jørgensen, U. G., et al. 2009, Monthly Notices of the Royal Astronomical Society, 396, 1023

Stassun, K. G., Collins, K. A., & Gaudi, B. S. 2017, The Astronomical Journal, 153, 136

Stassun, K. G., & Torres, G. 2018, The Astrophysical Journal, 862, 61

Stassun, K. G., Oelkers, R. J., Pepper, J., et al. 2018, The Astronomical Journal, 156, 102

Sullivan, P. W., et al. 2015, ApJ, 809, 77

Szabó, G. M., Pál, A., Derekas, A., et al. 2012, Monthly Notices of the Royal Astronomical Society, 421, L122

Szabó, G. M., Simon, A., & Kiss, L. L. 2014, Monthly Notices of the Royal Astronomical Society, 437, 1045

Thompson, S., et al. 2013, Kepler Data Release 19 Notes Q14, KSCI-19059-001, https://archive.stsci.edu/kepler/release_notes/release_notes19/DataRelease_19_20130204.pdf

Torres, G., Andersen, J., & Giménez, A. 2010, Astronomy and Astrophysics Review, 18, 67

Tregloan-Reed, J., Southworth, J., Burgdorf, M., et al. 2015, Monthly Notices of the Royal Astronomical Society, 450, 1760

Triaud, A. H. M. J., Collier Cameron, A., Queloz, D., et al. 2010, Astronomy and Astrophysics, 524, A25

Triaud, A. H. M. J., Neveu-VanMalle, M., Lendl, M., et al. 2017, Monthly Notices of the Royal Astronomical Society, 467, 1714

Urban, S., & Seidelmann, P. 2012, Explanatory Supplement to the Astronomical Almanac (University Science Books)

Wahl, S. M., Hubbard, W. B., & Militzer, B. 2016, The Astrophysical Journal, 831, 14

Walt, S. v. d., Colbert, S. C., & Varoquaux, G. 2011, Computing in Science & Engineering, 13, 22

Watson, C. A., & Marsh, T. R. 2010, Monthly Notices of the Royal Astronomical Society, 405, 2037

Weinberg, N. N., Sun, M., Arras, P., & Essick, R. 2017, The Astrophysical Journal Letters, 849, L11

Welsh, W. F., Orosz, J. A., Short, D. R., et al. 2015, The Astrophysical Journal, 809, 26

Wheatley, P. J., West, R. G., Goad, M. R., et al. 2018, Monthly Notices of the Royal Astronomical Society, 475, 4476

Wilkins, A. N., Delrez, L., Barker, A. J., et al. 2017, The Astrophysical Journal Letters, 836, L24

Wilson, D. M., Gillon, M., Hellier, C., et al. 2008, The Astrophysical Journal Letters, 675, L113

Winn, J. N. 2010, Exoplanets, 55

—. 2013, TESS Science Memo No. 1, Version 2. Available upon request.

Winn, J. N., Holman, M. J., Carter, J. A., et al. 2009, The Astronomical Journal, 137, 3826

Zahn, J.-P. 1977, Astronomy and Astrophysics, 500, 121

Zhou, G., Bayliss, D. D. R., Kedziora-Chudczer, L., et al. 2015, Monthly Notices of the Royal Astronomical Society, 454, 3002

APPENDIX

A. VERIFYING THE TESS TIME STAMPS

An obvious concern that one might have about the WASP-4 timing anomaly is that there might be a systematic offset between the TESS time system and the time system in which the previous observations have been reported. There is a precedent for this type of error: data from the Kepler mission was afflicted by a systematic timing error that was corrected only late in the mission (Thompson et al. 2013, Section 3.4). We performed two checks on the calibration of the TESS time system, described below.

A.1. *Checking for consistency in the headers of the lightcurve files*

The TESS lightcurve files provide observation start and end times in three different time systems: JD_{UTC}, JD_{TDB}, and BJD_{TDB}. First, we verified for a few select lightcurve files that JD_{UTC} lagged behind JD_{TDB} by the expected $32.184 + N$ seconds, where N is the number of leap-seconds since 1961. For the relevant observation time, $N = 37$, and the offset was as expected. Then, using the JD_{UTC} timestamp, we calculated the barycentric correction using the software written by Eastman et al. 2010. (For simplicity, we assumed the TESS spacecraft was located at the Earth's geocenter, because the light-travel time between the geocenter and the spacecraft is on the order of only one second.) This gave us times in BJD_{TDB} that agreed with the BJD_{TDB} times that are delivered with the TESS data products.

A.2. *Checking for timing anomalies in other hot Jupiter systems*
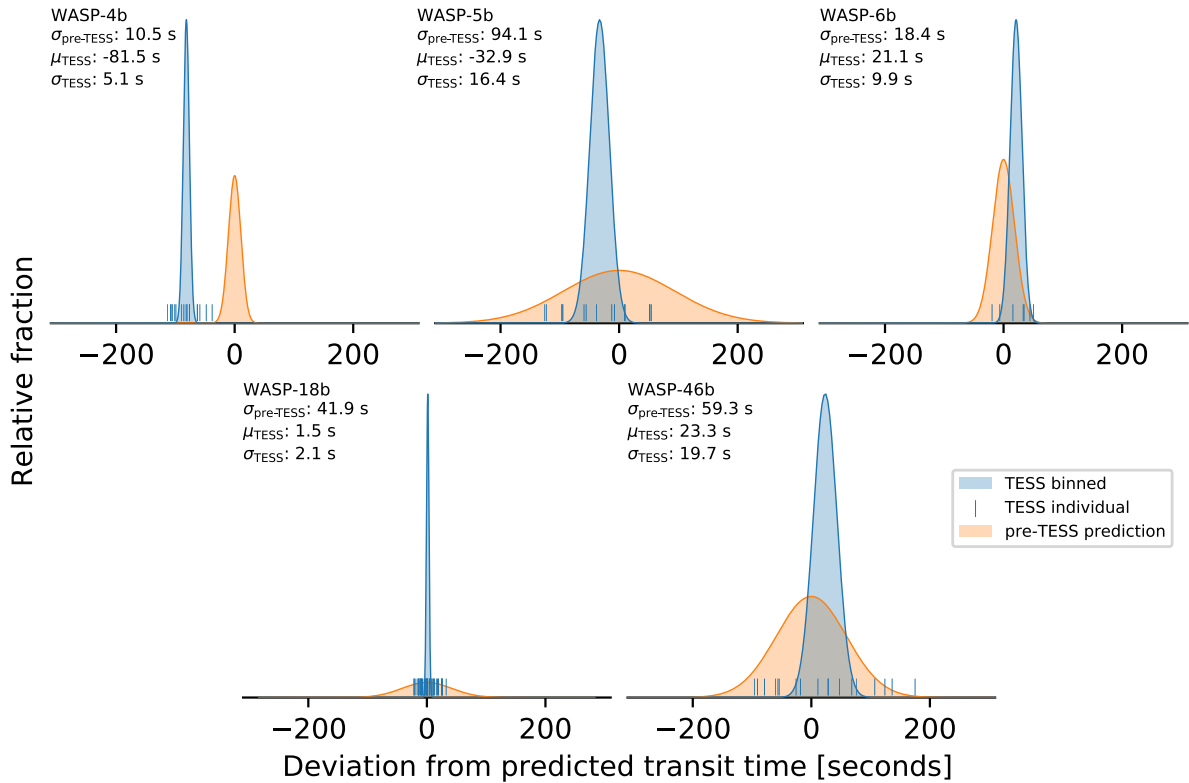
Figure 7. There is no evidence for a systematic offset between TESS times and the barycentric reference. While the WASP-4b transits fell about 82 seconds earlier than expected, other well-observed hot Jupiters, in particular WASP-6b and WASP-18b, arrived on time. Ticks are observed TESS transit midtimes; the orange distribution is a gaussian centered on zero with standard deviation ($\sigma_{predicted}$) calculated from the pre-TESS transit times. The blue distribution is a gaussian centered on the weighted average of the TESS times, with width equal to the uncertainty in the mean, *i.e.*, the standard deviation of the TESS residual times divided by $\sqrt{N-1}$, with N the number of transits.

If the observed timing delay in WASP-4b were caused by a systematic global offset between the TESS time system and the BJD_{TDB} reference, we would expect that it would be apparent in other hot Jupiter systems, too. It would also be apparent in

eclipsing binary observations and any other periodic phenomena that have been observed over a long time baseline. Here we examine only hot Jupiters because of our greater familiarity with the data.

We repeated all the data reduction and analysis steps described in this paper for other hot Jupiters observed by TESS for which timing data exists spanning many years. First, we checked which hot Jupiters were observed over the first three TESS sectors using a combination of `tessmaps`[4] and TEPCat (Southworth 2011). We then selected hot Jupiters for which there were at least five distinct epochs reported in the peer-reviewed literature. We required that each observation be of a single transit, that the midpoint be fit as a free parameter, and that the time system be clearly documented. Our final hot Jupiter sample included WASP-4b, 5b, 6b, 18b, and 46b. The collected and measured times are given in Tables 5, 6, 7, and 8 for each.

We determined the best-fitting constant-period ephemeris based on the pre-TESS data. Then we used the parameters and uncertainties in the best-fitting model to calculate the predicted transit times during the TESS observation period, as well as the uncertainty in the predicted times. The uncertainties are 11, 94, 18, 42, and 59 seconds for WASP-4b, 5b, 6b, 18b, and 46b, respectively. By comparing the observed and predicted times, Figure 7 shows that WASP-4b is the only hot Jupiter that transited significantly earlier than expected.

To use these results to place a quantitative limit on any global clock offset, for each hot Jupiter we considered the model

$$t_{\mathrm{tra}}(E) = t_0 + PE + t_{\mathrm{offset}},\tag{A1}$$

for t_{offset} a systematic constant offset between the reported timestamps and the true $\mathrm{BJD_{TDB}}$ reference. Our priors were

$$t_0 \sim \mathcal{N}[t_0', \sigma_{t_0'}],\tag{A2}$$

$$P \sim \mathcal{N}[P', \sigma_{P'}],\tag{A3}$$

$$t_{\mathrm{offset}} \sim \mathcal{U}[-20\sigma_{t_0'}, 20\sigma_{t_0'}],\tag{A4}$$

where $\mathcal{N}$ and $\mathcal{U}$ denote a normal and uniform distribution, (t_0', P') are the best-fit reference time and period using only the pre-TESS transit times, and $(\sigma_{t_0'}, \sigma_{P'})$ are the corresponding uncertainties.

For each planet, we asked: what fraction of the posterior for t_{offset} is consistent with an offset worse than 81.5 seconds? For WASP-4b, the answer is unsurprisingly 50%. For WASP-6b, the most constraining object, about 1 sample in 2 million is consistent with such a timing offset (4.9σ). For WASP-18b, 1 in 103 samples would be consistent with this timing offset (2.3σ), and in WASP-46b, the limit is 1 in 49 samples (2.0σ). For WASP-5b, the predicted time is too imprecise to rule out timing offsets at the necessary amplitude. Multiplying the three independent probabilities for WASP-5b, 6b, and 18b, we can rule out $t_{\mathrm{offset}} < -81.5$ seconds at 6.4σ, or about about 1 part in 11 billion.

Table 5. WASP-5b transit times, uncertainties, and references.

t_{tra} [BJD$_{\mathrm{TDB}}$]	$\sigma_{t_{\mathrm{tra}}}$ [days]	Epoch	Reference
2454383.76750	0.00040	-885	Anderson et al. (2008)
2454387.02275	0.00100	-883	Anderson et al. (2008)
2454636.17459	0.00082	-730	Fukui et al. (2011)
2454699.68303	0.00041	-691	Hoyer et al. (2012)
2454707.82465	0.00052	-686	Hoyer et al. (2012)
2454707.82523	0.00025	-686	Southworth et al. (2009)
2454730.62243	0.00031	-672	Southworth et al. (2009)
2454730.62301	0.00076	-672	Hoyer et al. (2012)
2454761.56356	0.00047	-653	Hoyer et al. (2012)
2454772.96212	0.00075	-646	Fukui et al. (2011)
2454774.59093	0.00030	-645	Hoyer et al. (2012)
2454787.61792	0.00069	-637	Hoyer et al. (2012)
2455005.82714	0.00036	-503	Hoyer et al. (2012)
2455049.79540	0.00080	-476	Hoyer et al. (2012)
2455075.84947	0.00056	-460	Dragomir et al. (2011)
2455079.10830	0.00079	-458	Fukui et al. (2011)

Table 5 continued

---

[4] github.com/lgbouma/tessmaps

Table 5 *(continued)*

$t_{\rm tra}$ [BJD$_{\rm TDB}$]	$\sigma_{t_{\rm tra}}$ [days]	Epoch	Reference
2455110.04607	0.00089	-439	Fukui et al. (2011)
2455123.07611	0.00079	-431	Fukui et al. (2011)
2455129.58759	0.00043	-427	Hoyer et al. (2012)
2455364.08150	0.00110	-283	Fukui et al. (2011)
2455377.10955	0.00093	-275	Fukui et al. (2011)
2455448.75927	0.00110	-231	Dragomir et al. (2011)
2456150.61479	0.00056	200	Moyano et al. (2017)
2456150.61396	0.00057	200	Moyano et al. (2017)
2458355.50829	0.00083	1554	This work
2458357.13741	0.00071	1555	This work
2458358.76412	0.00068	1556	This work
2458360.39377	0.00070	1557	This work
2458362.02273	0.00073	1558	This work
2458363.64908	0.00090	1559	This work
2458365.27827	0.00071	1560	This work
2458366.90627	0.00075	1561	This work
2458370.16411	0.00076	1563	This work
2458371.79126	0.00071	1564	This work
2458373.42123	0.00075	1565	This work
2458375.04910	0.00069	1566	This work
2458376.67856	0.00074	1567	This work
2458378.30530	0.00087	1568	This work
2458379.93419	0.00082	1569	This work

NOTE— $t_{\rm tra}$ is the measured transit midtime, and $\sigma_{t_{\rm tra}}$ is its 1σ uncertainty. The "Reference" column refers to the work describing the original observations. All the literature times except for the two Moyano et al. (2017) times are from the homogeneous Hoyer et al. (2012) analysis.

Table 6. WASP-6b transit times, uncertainties, and references.

$t_{\rm tra}$ [BJD$_{\rm TDB}$]	$\sigma_{t_{\rm tra}}$ [days]	Epoch	Reference
2454425.02167	0.00022	-398	Gillon et al. (2009a)
2455009.83622	0.00021	-224	Tregloan-Reed et al. (2015)
2455046.80720	0.00015	-213	Tregloan-Reed et al. (2015)
2455073.69529	0.00013	-205	Tregloan-Reed et al. (2015)
2455409.79541	0.00010	-105	Tregloan-Reed et al. (2015)
2455446.76621	0.00058	-94	Dragomir et al. (2011)
2455473.65439	0.00097	-86	Jordán et al. (2013)
2455846.72540	0.00045	25	Sada et al. (2012)
2456088.71801	0.00013	97	Nikolov et al. (2015)
2456095.43974	0.00017	99	Nikolov et al. (2015)
2456132.41082	0.00017	110	Nikolov et al. (2015)
2458357.39410	0.00033	772	This work
2458360.75573	0.00033	773	This work
2458364.11691	0.00032	774	This work
2458370.83872	0.00033	776	This work
2458374.19952	0.00031	777	This work
2458377.56026	0.00033	778	This work
2458380.92185	0.00038	779	This work

NOTE— $t_{\rm tra}$ is the measured transit midtime, and $\sigma_{t_{\rm tra}}$ is its 1σ uncertainty. The "Reference" column refers to the work describing the original observations.

Table 7. WASP-18b transit times, uncertainties, and references.

$t_{\rm tra}$ [BJD$_{\rm TDB}$]	$\sigma_{t_{\rm tra}}$ [days]	Epoch	Reference
2454221.48163	0.00038	-4037	Hellier et al. (2009)
2455221.30420	0.00010	-2975	Maxted et al. (2013)
2455432.18970	0.00010	-2751	Maxted et al. (2013)
2455470.78850	0.00040	-2710	Maxted et al. (2013)
2455473.61440	0.00090	-2707	Maxted et al. (2013)
2455554.57860	0.00050	-2621	Maxted et al. (2013)
2455570.58400	0.00048	-2604	Maxted et al. (2013)
2455876.55590	0.00130	-2279	Maxted et al. (2013)
2456896.14780	0.00080	-1196	Wilkins et al. (2017)
2457255.78320	0.00030	-814	Wilkins et al. (2017)
2457319.80100	0.00039	-746	Wilkins et al. (2017)
2458354.45782	0.00016	353	This work
2458355.39933	0.00015	354	This work
2458356.34070	0.00018	355	This work
2458357.28229	0.00018	356	This work
2458358.22348	0.00018	357	This work
2458359.16523	0.00020	358	This work
2458360.10661	0.00017	359	This work
2458361.04810	0.00017	360	This work

Table 7 continued

Table 7 *(continued)*

t_{tra} [BJD$_{TDB}$]	$\sigma_{t_{tra}}$ [days]	Epoch	Reference
2458361.98968	0.00016	361	This work
2458362.93130	0.00018	362	This work
2458363.87267	0.00018	363	This work
2458364.81374	0.00017	364	This work
2458365.75525	0.00019	365	This work
2458366.69709	0.00018	366	This work
2458369.52128	0.00017	369	This work
2458370.46281	0.00017	370	This work
2458371.40407	0.00017	371	This work
2458372.34537	0.00018	372	This work
2458373.28728	0.00018	373	This work
2458374.22818	0.00016	374	This work
2458375.16977	0.00017	375	This work
2458376.11132	0.00018	376	This work
2458377.05267	0.00017	377	This work
2458377.99444	0.00018	378	This work
2458378.93573	0.00016	379	This work
2458379.87722	0.00017	380	This work
2458380.81889	0.00018	381	This work
2458386.46729	0.00016	387	This work
2458387.40888	0.00017	388	This work
2458388.35021	0.00016	389	This work
2458389.29161	0.00015	390	This work
2458390.23334	0.00016	391	This work
2458391.17452	0.00016	392	This work
2458392.11593	0.00016	393	This work
2458393.05748	0.00015	394	This work
2458393.99898	0.00016	395	This work
2458394.94024	0.00017	396	This work
2458396.82309	0.00015	398	This work
2458397.76450	0.00015	399	This work
2458398.70656	0.00016	400	This work
2458399.64748	0.00015	401	This work
2458399.64748	0.00015	401	This work
2458400.58898	0.00017	402	This work
2458401.53083	0.00016	403	This work
2458402.47209	0.00017	404	This work
2458403.41360	0.00016	405	This work
2458404.35492	0.00017	406	This work

NOTE— t_{tra} is the measured transit midtime, and $\sigma_{t_{tra}}$ is its 1σ uncertainty. The "Reference" column refers to the work describing the original observations. All the literature times are from the homogeneous Wilkins et al. (2017) analysis.

Table 8. WASP-46b transit times, uncertainties, and references.

t_{tra} [BJD$_{TDB}$]	$\sigma_{t_{tra}}$ [days]	Epoch	Reference
2455396.60785	0.00062	-673	Anderson et al. (2012)
2455449.53082	0.00026	-636	Anderson et al. (2012)
2455722.73178	0.00023	-445	Ciceri et al. (2016b)
2455757.06195	0.00094	-421	Petrucci et al. (2018)

Table 8 continued

Table 8 *(continued)*

t_{tra} [BJD$_{TDB}$]	$\sigma_{t_{tra}}$ [days]	Epoch	Reference
2455858.61833	0.00009	-350	Ciceri et al. (2016b)
2456108.92771	0.00094	-175	Petrucci et al. (2018)
2456111.79422	0.00016	-173	Ciceri et al. (2016b)
2456111.79413	0.00012	-173	Ciceri et al. (2016b)
2456111.79424	0.00015	-173	Ciceri et al. (2016b)
2456130.38895	0.00042	-160	Petrucci et al. (2018)
2456131.81456	0.00112	-159	Petrucci et al. (2018)
2456194.75916	0.00027	-115	Ciceri et al. (2016b)
2456217.64127	0.00015	-99	Ciceri et al. (2016b)
2456217.64156	0.00013	-99	Ciceri et al. (2016b)
2456227.65574	0.00060	-92	Petrucci et al. (2018)
2456407.88096	0.00015	34	Ciceri et al. (2016b)
2456407.88085	0.00018	34	Ciceri et al. (2016b)
2456407.88148	0.00028	34	Ciceri et al. (2016b)
2456407.88159	0.00043	34	Ciceri et al. (2016b)
2456460.80526	0.00017	71	Ciceri et al. (2016b)
2456460.80450	0.00024	71	Ciceri et al. (2016b)
2456460.80547	0.00064	71	Ciceri et al. (2016b)
2456510.86818	0.00060	106	Petrucci et al. (2018)
2456510.86699	0.00015	106	Petrucci et al. (2018)
2456516.58667	0.00119	110	Petrucci et al. (2018)
2456520.88012	0.00064	113	Petrucci et al. (2018)
2456533.75260	0.00071	122	Ciceri et al. (2016b)
2456533.75480	0.00015	122	Ciceri et al. (2016b)
2456576.66289	0.00109	152	Petrucci et al. (2018)
2456589.54197	0.00090	161	Petrucci et al. (2018)
2456609.56653	0.00043	175	Petrucci et al. (2018)
2456839.85440	0.00123	336	Petrucci et al. (2018)
2456862.74085	0.00048	352	Petrucci et al. (2018)
2456882.76566	0.00073	366	Petrucci et al. (2018)
2456885.62429	0.00053	368	Petrucci et al. (2018)
2456915.66040	0.00123	389	Petrucci et al. (2018)
2456942.83880	0.00078	408	Petrucci et al. (2018)
2456948.56384	0.00074	412	Petrucci et al. (2018)
2457274.68458	0.00184	640	Petrucci et al. (2018)
2457294.70886	0.00140	654	Petrucci et al. (2018)
2457550.74797	0.00031	833	Petrucci et al. (2018)
2457593.65692	0.00024	863	Petrucci et al. (2018)
2457600.80985	0.00039	868	Petrucci et al. (2018)
2457610.82286	0.00020	875	Petrucci et al. (2018)
2458326.00972	0.00091	1375	This work
2458327.43899	0.00093	1376	This work
2458328.86970	0.00094	1377	This work
2458330.29965	0.00105	1378	This work
2458331.73234	0.00105	1379	This work
2458333.15977	0.00086	1380	This work
2458334.59230	0.00095	1381	This work
2458336.02222	0.00082	1382	This work
2458337.45111	0.00099	1383	This work
2458340.31143	0.00093	1385	This work
2458341.74347	0.00093	1386	This work
2458343.17362	0.00093	1387	This work
2458344.60303	0.00110	1388	This work
2458346.03436	0.00091	1389	This work

Table 8 continued

Table 8 *(continued)*

t_{tra} [BJD$_{\mathrm{TDB}}$]	$\sigma_{t_{\mathrm{tra}}}$ [days]	Epoch	Reference
2458347.46335	0.00168	1390	This work
2458348.89621	0.00086	1391	This work
2458350.32672	0.00101	1392	This work
2458351.75486	0.00103	1393	This work

NOTE— t_{tra} is the measured transit midtime, and $\sigma_{t_{\mathrm{tra}}}$ is its 1σ uncertainty. The "Reference" column refers to the work describing the original observations. All the literature times are from the homogeneous Petrucci et al. (2018) analysis. 14 of the lightcurves were acquired by ETD observers (see Petrucci et al. 2018).